Hygrothermal transfers through a bio-based multilayered wall – Modeling study of different wall configurations subjected to various climates and indoor cyclic loads

N. Reuge[1,*], F. Collet[1], S. Pretot[1], S. Moisette[1], M. Bart[1], O. Style[2], A. Shea[3], C. Lanos[1]

[1]Université de Rennes, Laboratoire de Génie Civil et Génie Mécanique, Axe Matériaux pour l'éco-construction, 3 rue du Clos Courtel, BP bb90422, 35704 Rennes, France

[2]Praxis Resilient Buildings, Ramon Turró 100-104, 5-7, 08005 Barcelona, Spain

[3]Department of Architecture & Civil Engineering, BRE Centre in Innovative Construction Materials, University of Bath, United Kingdom

*Corresponding author, e-mail: reuge@free.fr – phone: +33 6 01 90 15 78

Abstract

A bio-based multi-layered reference wall has been designed and tested. One of the key points of the research investigations was to be able to perform proper simulations of the hygrothermal transfers occurring inside the defined wall solutions. In previous work, the case of the reference wall subjected to a given real climate (Wroughton HIVE demonstrator, UK, Feb 2018) has been investigated. The present work, focused on the moisture regulation capacity of the wall, considers an improved kinetics model of sorption, different layer configurations, one additional climate (Bordeaux, FR, Apr 2008) and the effect of indoor cyclic loads. Compared to the classical approach, the local kinetics approach results in prediction of stronger and steeper relative humidity dynamics at small time scales. The study of the different wall configurations allows to determine the best one in terms of moisture damping: the vapor control membrane (Proclima INTELLO) is advantageously removed provided the OSB3 12 mm layer is replaced by an OSB4 18 mm layer. Moreover, the simulations show that the Moisture Buffer Value characteristic of the material layer is not a sufficient criterion to evaluate hygric performance; strong interactions occur with its permeability independently of its sorption capacity. Finally, water content hysteresis phenomena are studied and it appears that under some usual operating conditions, they can be ignored in preference to adjust the layers' permeabilities to adequate fits on the Moisture Buffer Value tests.

Keywords

Bio-based building materials; Local kinetics of sorption; Hygrothermal transfer; Moisture regulation; Modeling

1 Introduction

In the framework of the European ISOBIO project (featuring the slogan "naturally high-performance insulation"), several research teams and manufacturers have worked together to develop bio-based solutions for the building industry. Among these solutions, the most innovative one consisted of an exclusive bio-based multilayered wall for new buildings. The bio-based materials that have been developed involve very low carbon footprints and high insulating properties.

This study is focused on this bio-based multilayered reference wall. In previous investigations, proper simulations of the hygric and heat transfers occurring inside this reference wall have been carried out: by Reuge et al. studying the ISOBIO reference wall submitted to a real climate (Reuge et al., 2020a and

2020b) or in the controlled environment of a bi-climatic room (Reuge et al., 2020c). The present work goes further in numerically testing several variants of wall configuration, all based on the bio-based materials developed in this framework, and in different climates in order to enhance the moisture regulation capacity of the wall.

Bio-based materials classically have good insulating properties. Moreover, they are usually excellent moisture regulators as shown in Abbas et al. (2020), Dhakal et al. (2017), Douzane et al. (2016) and Fu et al. (2021). In their experimental and modeling study, Mnasri et al. (2020) proved the ability of bio-based materials (and more particularly a wood-cement composite) to improve hygrothermal comfort and buildings energy consumption. The capacity of moisture regulation is the property that will be particularly investigated in this study.

Moisture regulation depends on water sorption (adsorption and desorption) phenomena occurring within the porous materials. Classically, the exchanges between water vapor and adsorbed water are described by the equilibrium sorption isotherms also called "water storage functions". They can be experimentally determined by gravimetric methods (Iglesias and Chirife, 1982). Adsorption and desorption isotherms can be significantly different and this involves hysteretic phenomena depending on the materials' hygric histories (Costantine, 2020); they can be described by hysteretic models as described in Carmeliet et al. (2005) or in Huang et al. (2005). Taking this into consideration, conventional approaches are still based on the assumption that for a given local relative humidity φ, the corresponding equilibrium local water content w is reached instantaneously, such as in the so-called Künzel approach (Künzel, 1995). However, these models are not able to provide a good description of the transient hygric state in these porous media. This has been shown for bio-based materials: in Nyman et al. (2006) for cellulosic materials, in Frandsen et al. (2007) and Eitelberger and Svensson (2012) for wood, in Alexanderson et al. (2016) for paperboard, in Challansonnex et al. (2019a, 2019b) for fiberboards and wood, by Reuge et al. (2020a, 2020b, 2020c) for ISOBIO materials and in Reuge et al. (2019) for various hemp-lime concretes – but also for more classic compounds such as cements in Johannesson and Nyman (2010) and Janssen et al. (2016). In the previous studies of Reuge et al. (2019, 2020a, 2020b, 2020c) various bio-based materials were studied and it was demonstrated that the conventional approach led to patent inconsistencies such as underestimation of the relative humidity (*RH*) dynamics. Thus, as reported in the aforementioned literature, our previous studies have established that a local kinetics of sorption exists (from water vapor to adsorbed water and inversely) which can be slow compared to the diffusive phenomena. These deviations obtained from conventional models are of particular concern when the moisture regulation capacity is studied.

The numerical studies performed in the framework of the ISOBIO project are the first, to our knowledge, investigating a multilayered fully bio-based wall in real climatic conditions. Moujalled et al. (2018) have studied the effect of real climatic conditions (Périgueux, FR) on a bio-based building with a wall of three layers: a hemp-lime concrete but with classic internal and external renders. Their results confirmed that bio-based materials are good indoor climate regulators. Their simulations with hysteresis unexpectedly gave poorer results than without. Piot et al. (2015) have also studied a three-layered wall (Savoie, FR) in real climatic conditions: a hemp concrete but also with classic internal and external renders. Their study showed that a hempcrete wall is very sensitive to the moisture-related properties of the exterior coating. In various studies: Colinart et al. (2016a, 2017b), Fabbri and McGregor (2017), Lelievre et al. (2014), Rahim et al. (2016), and Seng et al. (2017), the authors have studied the response of hemp concrete panels to controlled indoor and outdoor conditions. Note that in most of the aforementioned literature, for instance in Rahim et al. (2016), Colinart et al. (2017) and Fabbri and McGregor (2017), it appears that the simulations based on the classical Künzel approach systematically underestimate the small time scales *RH* dynamics.

The first part of this study presents the studied wall and variant configurations and then gives a summary of the classic hygric and thermal properties obtained from characterizations performed on samples of ISOBIO materials. Then, the theoretical background required to model the water sorption under the assumption of a slow kinetics is presented, relying on previous studies (Reuge et al., 2020a, 2020b, 2020c). The last part presents the numerical investigations and comparisons with experiments over a wide range of hygric and thermal operating conditions: first Moisture Buffer Value (MBV) tests are studied, then the reference wall and variant configurations submitted to various climates (Wroughton, UK – HIVE demonstrator – Feb 2018 and Bordeaux, FR – Apr 2008) and indoor cyclic loads and finally the role of hysteresis phenomena are studied.

2 ISOBIO multilayered wall and classic hygrothermal properties of the layers

2.1 Reference ISOBIO wall and variants

The ISOBIO reference wall is composed of: a lime-hemp render (BCB, from BCB™), a Rigid insulation panel made of hemp shiv and an organic binder (CAV, from CAVAC™), flexible insulation panels made of hemp flax and cotton (BIO1 & BIO2, Biofib Trio from CAVAC™), an OSB3 panel, a INTELLO membrane (INT, from Proclima™), a panel made of compressed straw (CSB, Lignicell from CSB™) and a clay-hemp plaster (CLA, from CLAYTEC™). Note that this wall is supported by a timber frame which will not be considered in the simulations. The configuration and the thicknesses of the different layers are given in Figure 1.

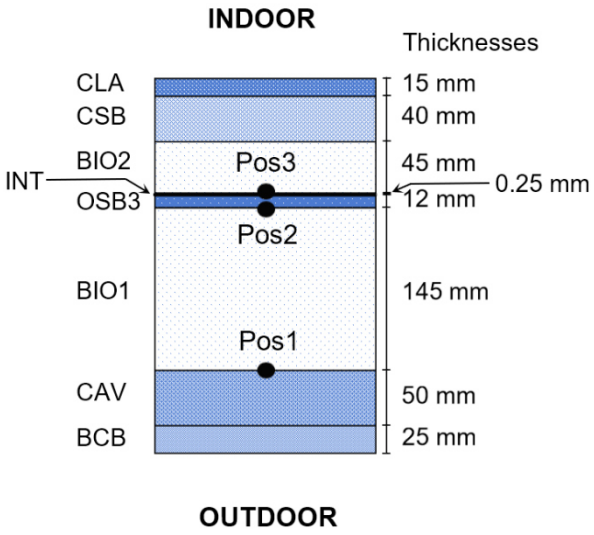

Figure 1: ISOBIO reference wall

This reference wall configuration will be referred to WCONF1. Then, three variants of this reference configuration will be studied:

- WCONF2: the INTELLO membrane is removed, the other layers remaining the same as WCONF1,

- WCONF3: the INTELLO membrane is removed, OSB3 12 mm is replaced by OSB4 18 mm, the other layers remaining the same as WCONF1,

- WCONF4: the INTELLO membrane is removed, OSB3 12 mm is replaced by OSB4 18 mm and the Lignicell CSB panel 40 mm is replaced by the CAVAV Rigid panel 50 mm, the other layers remaining the same as WCONF1.

The removal of INT will result in an enhanced circulation of vapor between the internal layers (BIO2, CSB, CLA) and the external layers (BCB, CAV, BIO1, OSB3) allowing the external layers to work as moisture regulators from the point of view of the internal layers. However, without INT, the air tightness of the wall will be reduced too much and this is why OSB3 12 mm is replaced by OSB4 18 mm in WCONF3 (note that it will also allow to reinforce the vapor resistance of the wall). Finally, CAV being a better hygric regulator than CSB (with a MBV of 1.7 against 0.77 g/(m².%*RH*), (Collet et al., 2019)), CSB is replaced by CAV in WCONF4.

2.2 Hygrothermal properties and models of properties

Table 1 synthesizes the classic hygrothermal properties of the constitutive materials of the ISOBIO wall. It is a compilation of the properties necessary to perform the simulations: the bulk densities at dry state ρ_0, the open porosities ε_0, the vapor diffusion resistance factors at dry state μ_0, the thermal conductivities at dry state λ_0 and the specific heat capacities at dry state Cp_0. Note that while most of these properties have been determined in Collet et al. (2019) a few others come from trustable technical sheets. Note that for OSB4, the same properties and models of properties as OSB3 have been used, except μ_0 which is considered equal to 300 (*cf*. F-IBP database and technical sheets) instead of 138 for OSB3.

	ρ_0 (kg.m^{-3})	ε_0 (-)	μ_0 (-)	λ_0 (W.m^{-1}.K^{-1})	Cp_0 (J.kg^{-1}.K^{-1})
BCB	530	0.546	9	0.13	1006
CAV	190	0.874	11	0.07	2100
BIO	26.5	0.98	3.6	0.039	1800
OSB3	551	0.609	138	0.13	1600
OSB4	551	0.609	300	0.13	1600
INT	85	0.085	$1.364.10^5$	2.4	2500
CSB	449	0.72	27	0.10	1700
CLA	1392	0.294	10	0.62	1040

Table 1: ISOBIO materials properties at dry state, T = 23°C

The adsorption isotherm of representative samples of the ISOBIO materials (CAV, BIO, OSB3 and CSB) have been studied in Collet et al. (2019). The moisture storage functions of the other ISOBIO materials come from trustworthy technical sheets and / or F-IBP databases (BCB, INT and CLA).

Note that, in the equations, the local hygric variables given at the macroscopic scale will be written as lower case letters (*e.g*. the local water content w, the local relative humidity φ) while the hygric variables given at the sample scales will be written as upper case (*e.g*. the global water content W, the global relative humidity RH).

The appropriate models of properties needed for the simulations have been studied in (Reuge et al., 2020a). For the isotherms of adsorption, the Van Genuchten model VG (Van Genuchten, 1980) has been used. It is expressed as follows:

$$W_{eq}\left(RH\right) = W_{\text{sat}}\left[1+\left(-h\ln\left(RH\right)\right)^{\eta}\right]^{1/\eta-1} \quad (1)$$

where h and η are adjustment coefficients. The values of these adjustment coefficients are given in Table 2 and the isotherms of adsorption of CAV and CSB are shown in Figure 2 at a temperature of 23°C. Note that the CAV desorption isotherm given in Table 2 and in Figure 2 is not based on experimental data but on considerations that will be discussed in section 4.2.

The evolution of the vapor diffusion resistance factor μ of the Proclima INTELLO membrane must be taken into account because it is a humidity-variable material, its value of μ evolves strongly as a function of *RH*: from 550 at 100% *RH* to 136400 at 0% *RH*. The data provided by Proclima / F-IBP have been fitted by a logistic power law (Reuge et al., 2020a), *i.e.*, $\mu = 1/\left(7.33\,10^{-6} + 1.8.10^{-3}.\varphi^{7.644}\right)$.

Finally, the evolution of the thermal conductivities as a function of the water content has been modeled by the self-consistent scheme (Collet and Pretot, 2014), which takes the following expression:

$$\lambda(W) = \lambda_s \left\{1 + \varepsilon_0 \left[(1-\varepsilon_0)/3 + \left(3 + (W/1000\varepsilon_0)(\lambda_a/\lambda_w - 1)\right) \cdot \left(3(\lambda_a/\lambda_s - 1) - (W/1000\varepsilon_0)(\lambda_a/\lambda_w - 1)\left(2\lambda_w/(\lambda_s + 1)\right)\right)^{-1} \right]^{-1} \right\} \quad (2)$$

where λ_a (0.025 W.m^{-1}.K^{-1}) is the air thermal conductivity and λ_w (0.6 W.m^{-1}.K^{-1}) is the liquid water thermal conductivity. The coefficients λ_s have been adjusted such as $\lambda(W=0)$ equals λ_0. The values of λ_s are given in Table 2.

Expressions (1) and (2) are written at the sample scale but they remain valid at the local macroscopic scale replacing *RH* by φ and *W* by *w*.

		W_{sat} (kg.m^{-3})	h (-)	η (-)	λ_s (W.m^{-1}.K^{-1})
BCB		546	8524	1.38	0.312
CAV	Adsorption	874	27490	1.435	0.53
	Desorption	874	10^5	1.35	
BIO		348	228504	1.473	1.055
OSB3		609	11360	1.325	0.367
OSB4		609	11360	1.325	0.367
INT		85	2091	1.42	2.74
CSB		720	23172	1.334	0.38
CLA		294	271	1.656	0.995

Table 2: Adjustment coefficients – VG model and self-consistent scheme (T = 23°C)

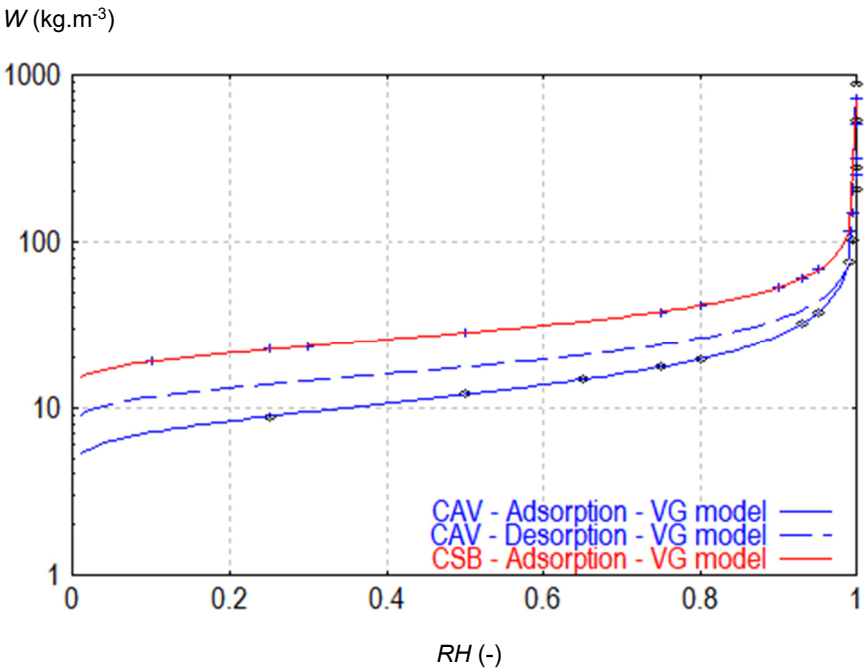

Figure 2: Isotherms of adsorption of CAV and CSB ISOBIO materials at T = 23°C – Experimental data (symbols) and adjustments with the VG model (lines)

2.3 Wall thermal transmittances and vapor resistances

Based on the materials' thermal conductivities λ_0 and vapor diffusion resistance factors μ_0 at dry state, the total thermal transmittance U and vapor resistance R of these walls are shown in Table 3 for the four configurations. As can be seen, the replacement of CSB by CAV (WCONF4) results in a slightly lower U, the removal of INT (WCONF2) results in a very significantly lower R but the replacement of OSB3 by OSB4 allows to regain some vapor resistance (WCONF3 and WCONF4).

Wall configuration	U (W.m^{-2}.K^{-1})	R (Pa.m^2.s.kg^{-1})
WCONF1	0.155	$1.95.10^{11}$
WCONF2	0.155	$2.21.10^{10}$
WCONF3	0.154	$4.11.10^{10}$
WCONF4	0.147	$3.84.10^{10}$

Table 3: Total thermal transmittances U and vapor resistances R

Note that a sensitivity study of λ_0 and μ_0 of the different layers on U and R has been performed on the reference wall (WCONF1) in Reuge et al. (2020a).

3 Hygrothermal transport: theoretical background

3.1 Mass transport governing equations

First, (*i*) air transport is ignored. In porous media, water is present in gaseous form (water vapor) and in liquid form (adsorbed water). Therefore, there are two mass balance equations to consider. Assuming that (*ii*) the convective transport is negligible, they take the following forms (Reuge et al., 2020a):

$$\begin{cases} \dfrac{\partial\left(\varphi P_{sat}\right)}{\partial t} - \nabla\cdot\left[\delta_{v,p}\dfrac{RT}{M_w}\nabla\left(\varphi P_{sat}\right)\right] = -\dfrac{RT}{M_w}R_s \\ \dfrac{\partial w}{\partial t} - \nabla\cdot\left(D_{l,p}\nabla w\right) = R_s \end{cases} \quad (3,4)$$

where the porous media vapor permeability is: $\delta_{v,p} = \delta_v/\mu = D_v M_w/\mu RT$, the water vapor diffusion resistance factor being given by: $\mu = \delta_v/\delta_{v,p} = D_v/D_{v,p}$, $D_{v,p}$ and $D_{l,p}$ are the water vapour and liquid water diffusivities in the porous media respectively. R_s is the local sorption rate which will be detailed in section 3.3.1.

The hysteretic behavior can be handled by the model of Huang et al. (2005): it has been validated for hemp concrete by Oumeziane et al. (2014). Here, reversal points (*i.e.*, shifts from adsorption to desorption or inversely) occur when the sign of R_s changes.

As explained in the introduction, the classical assumption is that the rate of sorption R_s is very fast compared to the vapor diffusive flux. This is not the case for the bio-based materials studied here. According to this classical assumption, the following single governing equation can be obtained:

$$\left.\frac{\partial w}{\partial\varphi}\right|_T \frac{\partial\varphi}{\partial t} - \nabla\cdot\left[\left(\delta_{v,p}P_{sat} + D_{p,l}\left.\frac{\partial w}{\partial\varphi}\right|_T\right)\nabla\varphi\right] = 0 \quad (5)$$

Equation (5) is the so-called Künzel mass transfer equation (Künzel, 1995).

The classic heat transport governing equation is not given here but it is obviously taken into account considering latent heat of vaporization (Künzel, 1995).

3.2 Boundary conditions

At the wall or sample surface $surf_i$, the relative humidity is given by:

$$\varphi_{surf_i} = RH - \frac{\delta_{v,p}}{h_m}\cdot\nabla\varphi\big|_{surf_i} \quad (6)$$

where h_m is the mass transfer coefficient and the water content is given by:

$$\nabla w\big|_{surf_i} = \beta\left.\frac{\partial w}{\partial\varphi}\right|_T \nabla\varphi\big|_{surf_i} \quad (7)$$

where β is in the range of 0 to 1 and dynamically depends on the sorption rate R_s. Its value will be considered as a constant value of 1 which means that the sorption equilibrium is always reached at the wall surface. It was shown in Reuge et al. (2020a) that its value (0 or 1) does not significantly impact the simulation results.

3.3 Local sorption rate

3.3.1 Theory

As shown in Reuge et al. (2019, 2020a, 2020c), the sorption of water vapor to liquid water and vice-versa is not instantaneous as commonly assumed but follows local kinetics with a kinetic constant k_0 for each material. From Reuge et al. (2019, 2020a, 2020c), the sorption rate R_s is expressed as follows:

$$R_s = \pm k_0 \left(w_{eq}(\varphi) - w \right)^2 \quad (8)$$

where k_0 (day^{-1}/(kg.m^{-3})) is a kinetic constant of a second order kinetics. The sign in front of k_0 is the same as the sign of $\left(w_{eq}(\varphi) - w \right)$, *i.e*. plus for adsorption, minus for desorption.

From (Reuge et al., 2020c), this expression tends to underestimate the sorption rate at the very beginning of the sorption process, leading to the following improved expression:

$$R_s = k_0 \left(\pm 0.75 + 10^6 \frac{\partial \varphi}{\partial t} \right) \left(w_{eq}(\varphi) - w \right)^2 \quad (9)$$

Justifications and physical interpretations of models (8) and (9) have been discussed in previous studies. As explained in Reuge et al. (2020c), while the term $0.75 k_0 \left(w_{eq}(\varphi) - w \right)^2$ describes the slow diffusion of bound water molecules in the biological cells (Reuge et al., 2019), the new term $k_0 10^6 \frac{\partial \varphi}{\partial t}$ would describe the sudden capillary sorption of water in the macropores due to the Kelvin effect (Collet et al., 2008) occurring immediately during a sudden variation of local relative humidity φ.

3.3.2 Kinetic constants of the ISOBIO materials

From Reuge et al. (2020a, 2020c), the kinetics constants k_0 have been determined adjusting simulations on sorption experiments by inverse method. Their values are very different according to the material: from 0.15 day^{-1}/(kg.m^{-3}) for BCB to about 14 day^{-1}/(kg.m^{-3}) for BIO, *i.e*. a difference of 2 orders of magnitude. Regarding CAV, as shown in Reuge et al. (2020a), k_0 is a constant value of 0.3 day^{-1}/(kg.m^{-3}) in the 20-70% *RH* range but decreases for higher *RH*: in the 80-95% *RH* range, the value of k_0 is of about 0.1 day^{-1}/(kg.m^{-3}). Table 4 compiles the values of k_0 considered in this study (for the materials for which k_0 remains unknown, *i.e*. INT and CLA, a median value of 0.25 day^{-1}/(kg.m^{-3}) is considered; note that the thicknesses of the layers of these two materials in the reference ISOBIO wall are relatively small).

	k_0 (day^{-1}/(kg.m^{-3}))
BCB	0.15
CAV	0.1 - 0.3
BIO	14
OSB3	0.4
OSB4	0.4
INT	0.25*
CSB	0.25
CLA	0.25*

*Unknown, approximated as median value

Table 4: ISOBIO materials kinetic constants k_0 (Reuge et al., 2020a, 2020c)

3.4 Hysteresis model

The most advanced models describing hygric hysteresis phenomena in porous materials are those of Carmeliet (2005) and Huang et al. (2005). Both models describe the adsorption scanning curves with

the same shape parameters as those for the main adsorption curve. The same assumption is done for the desorption process.

In Oumeziane et al., (2014), both models have been adapted for building materials by using relative humidity instead of capillary suction. The authors used and compared them to measurements performed on hemp concretes. The model of Huang et al. (2005) has proved to be the most consistent with particularly good agreement with the measurements for the studied bio-based materials. Thus, in this study, only this last one has been considered (for the simulations presented in section 4.3.4.4). According to this model, after a series of alternating adsorption and desorption processes, adsorption and desorption scanning curves are given by:

$$w(\varphi,i) = w_r(i) + \left(w_s(i) - w_r(i)\right)\frac{w_{ads}(\varphi)}{w_{sat}} \tag{10}$$

where $w_r(i)$ and $w_s(i)$ are the residual and saturated water contents of the scanning curve indexed i. The main adsorption and desorption curves give residual and saturated water content values at order 0: $w_r(0) = 0$ and $w_s(0) = w_{sat}$. The calculation of these parameters is based on the perfect closure of the scanning curve at reversal points. Scanning curve indexed i includes the last reversal point (φ_i, w_i) and the penultimate reversal point (φ_{i-1}, w_{i-1}). Calculating $w_r(i)$ and $w_s(i)$ finally leads to solve a linear system of two equations (Oumeziane et al., 2014).

4 Simulations

4.1 Simulation tools

Two simulation tools based on the finite differences and developed under Matlab, have been used:

- TMC, a 1D Cartesian tool based on the classic approach of Künzel (Oumeziane, 2013),

- TMCKIN, a 1D Cartesian tool based on the local kinetics approach (Reuge et al., 2020a).

TMC considers a constant time step (5 min) whereas TMCKIN handles an adaptative time step (typically varying between 10^{-3} s and 10 s).

4.2 Adjustments of μ values by simulations of MBV tests

Simulations of the Moisture Buffer Value (MBV, Nordtest project's protocol by Rode et al., (2005)) tests had been performed and successfully adjusted on experiments by Reuge et al. (2020c). Here, the investigations on the CAV material go further performing a sensitivity study and considering hypothetic hysteretic effects. The operating conditions of MBV tests have to be recalled: the exposed surface of the studied material is subjected to several consecutive cycles of ambient hygrometry: 8 h at 75% *RH* / 16 h at 33% *RH* and so on. The results of these measurements for CAV and CSB are reproduced in Figure 3a and 3b.

Regarding the simulations, the liquid diffusivities $D_{l,p}$ were ignored since they are not known. Note that, in the field of bio-based materials, the determinations of these coefficients would involve extremely long interactions between permeability measurements and numerical simulations (*i.e.*, years of investigations, please see Oumeziane (2013). Thus, the common approach is to use the inverse method to adjust apparent vapor diffusion resistance factors μ. It is worth recalling that the permeability measurements lead to apparent μ as well. The limitation of this approach is that the liquid diffusive transport is ignored in favor of an apparent vapor diffusive transport. With this approach, the adjusted

values of μ are apparent data which are in principle between the measured values of μ_0 and the lower μ_{humid}; this is due to the increasing liquid diffusivity $D_{l,p}$ with *RH* in the physical reality (Oumeziane, 2013).

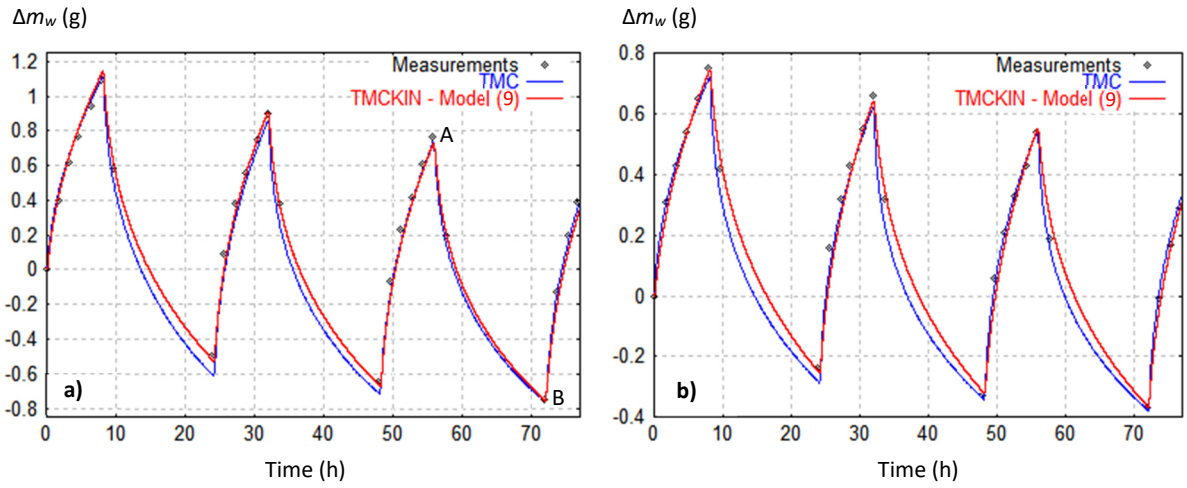

Figure 3: MBV tests – Temporal evolution of relative water mass in (a) the CAV sample and (b) the CSB sample – Measurements, TMC & TMCKIN simulations (Reuge et al., 2020c)

Then, a reflection about the mass transfer coefficient h_m at the exposed sample surface is necessary. During the MBV experiments, the air velocity in the vicinity of this surface is of about 0.1 m.s^{-1}. From in-depth studies: Mortensen et al. (2005) and Talev et al. (2012), the value of h_m for a smooth material in these operating conditions can safely be estimated in the range of $2{\cdot}10^{-8}$ to $3{\cdot}10^{-8}$ kg.m^{-2}.Pa^{-1}.s^{-1}. But taking into account the rugosity of the sample, a multiplication factor has to be considered: it is usually estimated to be about 1.5 or even 2 for concretes (Oumleziane, 2013). Thus, a value of h_m in the range of $3{\cdot}10^{-8}$ to $6{\cdot}10^{-8}$ kg.m^{-2}.Pa^{-1}.s^{-1} had to be considered. The MBV simulations performed by Reuge et al. (2020c) had considered a value of h_m of $4{\cdot}10^{-8}$ kg.m^{-2}.Pa^{-1}.s^{-1}.

The adjustments with TMCKIN had been performed using the improved local kinetics model (9), they were not possible using model (8) because the later underestimates the kinetics at short time scales as demonstrated in (Reuge et al., 2020c). The results of these simulations for CAV and CSB are reproduced in Figure 3a and 3b. The adjustment values of μ are of 5.5 and 27 respectively using TMCKIN and 6.75 and 40 respectively using TMC. The correlation coefficients are around 0.995 (Reuge et al., 2020c).

Then, a sensitivity study was performed for the CAV sample studying the effects of the variation of various parameters ($\delta_{v,p}$ or μ, k_0 and h_m) on the amplitudes of the relative water mass variations calculated by TMCKIN, more precisely on the position of points A and B in Figure 3a. The results are presented in Table 5: the sensitivity *S* of a given property *P* means that if this property is modified by *x*% in the range of [-Δ, +Δ], the predicted amplitude is modified by approximately (*S*.*x*)%.

According to Table 5, the sensitivity study reveals that $\delta_{v,p}$ (or μ) is the most sensitive parameter, followed by k_0 and finally by h_m. The strong sensitivity of μ is not a problem since this parameter is determined by adjustment, k_0 can be determined with sufficient accuracy but as explained previously the determination of the value of h_m is marked by a strong uncertainty.

Then, still regarding the CAV material, the MBV calculation (TMCKIN) has been performed considering hysteretic effects taking into account the desorption isotherm provided in Table 2 and Fig. 2. As a

result, the adjustment can be as good as the one reported in Fig. 3a adjusting the μ value (reduced by 18%, *i.e*. 4.5 instead of 5.5), the correlation coefficient then reaches 0.995.

Property P	$\frac{\text{Ampl.}_{AB} - \text{Ampl.}_{AB,ref}}{\text{Amplitude}_{AB,ref}}$ (%)	$S = \frac{\text{Ampl.}_{AB}(P+\Delta) - \text{Ampl.}_{AB}(P-\Delta)}{2\Delta \cdot \text{Amplitude}_{AB,ref}(P)}$ (-)
$\delta_{v,p}$ + Δ, Δ = 20% (*i.e.* μ - 17%)	7.51	0.38
$\delta_{v,p}$ – Δ, Δ = 20% (*i.e.* μ + 25%)	-8.83	0.44
k_0 + Δ, Δ = 50%	6.07	0.12
k_0 – Δ, Δ = 50%	-14.61	0.29
h_m + Δ, Δ = 50%	2.54	0.05
h_m – Δ, Δ = 50%	-7.17	0.14

Table 5: Results of the MBV sensitivity study (TMCKIN) in terms of Δm_w relative amplitudes between points A and B (of Fig. 3a) and sensitivity S – CAV material

Note that 4.5 corresponds to the measured value of μ_{humid} in Collet et al. (2019), this is with the intention that the proposed desorption isotherm has been conceived (a hysteretic behavior stronger than the one proposed here seems unlikely). Note that keeping μ of 5.5, a as good adjustment can also be obtained increasing h_m by 50%, *i.e*. $6 \cdot 10^{-8}$ instead of $4 \cdot 10^{-8}$ kg.m^{-2}.Pa^{-1}.s^{-1} (which is at the upper limit of the aforementioned range). Obviously, a good adjustment can also be obtained both increasing h_m and adjusting μ to lesser extents. These considerations may seem purely theoretical but they allow to show that taking into account the proposed desorption isotherm still can lead to consistent results using adequate adjustments.

In order to synthesize all these results, the different values of μ obtained from adjustments are reported in Table 6. As explained previously, the adjusted values of μ are apparent data which can be significantly lower to the measured values of μ_0 (especially for CAV) due to the increasing liquid diffusivity $D_{l,p}$ with *RH*. Regarding the values of μ_{TMCKIN} obtained for CAV, note that they remain greater or equal than the apparent value of μ "humid" measured in (Collet et al., 2019) (*i.e*., 4.5). Regarding the value of μ_{TMCKIN} obtained for CSB, note that it remains equal to the μ "dry" measured in Collet et al. (2019) (*i.e*., 27), suggesting that the liquid diffusivity in this fibrous material remains low in the considered range of *RH*.

	μ_{TMC} (-)	μ_{TMCKIN} (-)
CAV, adsorption (no hysteresis)	6.75	5.5
CAV, adsorption and desorption (hysteresis)	5.5	4.5
CSB, adsorption (no hysteresis)	40	27

Table 6: Values of μ obtained by adjustments of TMC & TMCKIN on the MBV tests – CAV material

4.3 Wall simulations

4.3.1 Assumptions

For the mathematical models, assumptions are given in section 3.1. Regarding the sorption isotherms, the measurements done in adsorption conditions at 23°C (Table 2, Fig. 2) have been used: consequently, temperature effects have been neglected. No hysteresis effect has been considered except in the last section (4.3.4.4) where it is studied. Vapor resistance factor coefficients at dry state μ_0 have been considered for BCB, BIO, OSB3, OSB4 and CLA (*cf*. Table 1), adjusted apparent vapor resistance factor coefficients μ_{TMC} and μ_{TMCKIN} from Table 6 have been considered for CAV and CSB to be consistent with the MBV tests. Regarding INT, μ as a function of *RH* according to the law given in section 2.2 was used. Liquid diffusive fluxes have been ignored.

For TMCKIN simulations, kinetics constants k_0 given in Table 3 have been considered. Since *RH* is above 80% in the CAV external layer, a value of k_0 of 0.1 $day^{-1}/(kg.m^{-3})$ was used.

4.3.2 Boundary conditions

In the framework of the ISOBIO project, the Wroughton measurements (HIVE demonstrator) have been performed during 18 days of winter 2018 (from 02/24 to 03/14), *i.e*. a duration of 432 hours. The demonstrator setup is described in Reuge et al. (2020a). During this period, the indoor and outdoor *T* and *RH* measurements are shown in Figures 4a and 4b respectively. As shown by these Figures, this climate was humid and cold, with outdoor *RH* varying between 50% and 100% and outdoor *T* varying between -7°C and 12°C. Solar radiation was measured (see Fig. 9 of Reuge et al., 2020a) and has been taken into account in the simulations, but wind and rain on outdoor boundary conditions have been ignored. Note that classic simulations (Künzel approach) had been performed with/without considering wind and rain and led to insignificant differences at the studied positions.

The second climate considered here corresponds to 18 days of the Bordeaux's climate of spring 2008 (from 04/08 to 04/26, source: Météo France), *i.e*. a duration of 432 hours. During this period, the indoor and outdoor *T* and *RH* measurements are shown in Figures 5a and 5b respectively, the indoor values are the same as considered above. As shown by these Figures 5a and 5b, this climate was rather humid and soft, with outdoor *RH* varying between 32% and 98% and outdoor *T* varying between 3°C and 20°C.

Therefore, these two climates are significantly different but they both show important *RH* and *T* variations. For the simulations, typical values have been considered for outdoor and indoor heat transfer coefficients, 17 and 8 $W.m^{-2}.K^{-1}$ respectively, see Erhorn and Szerman (1992) and Schaube and Werner (1986). For outdoor and indoor mass transfer coefficients, typical values of $7.4 \cdot 10^{-8}$ and $2.6 \cdot 10^{-8}$ $kg.Pa^{-1}.m^{-2}.s^{-1}$ have been considered respectively, see Erhorn and Szerman (1992) and Schaube and Werner (1986).

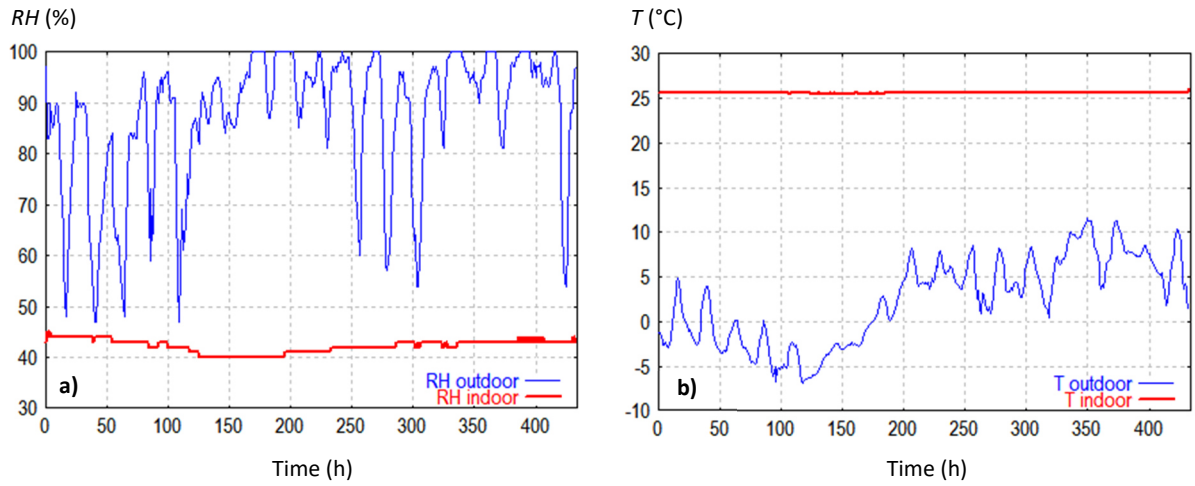

Figure 4: Wroughton measurements (HIVE demonstrator) – Indoor and outdoor *RH* (a) and *T* (b)

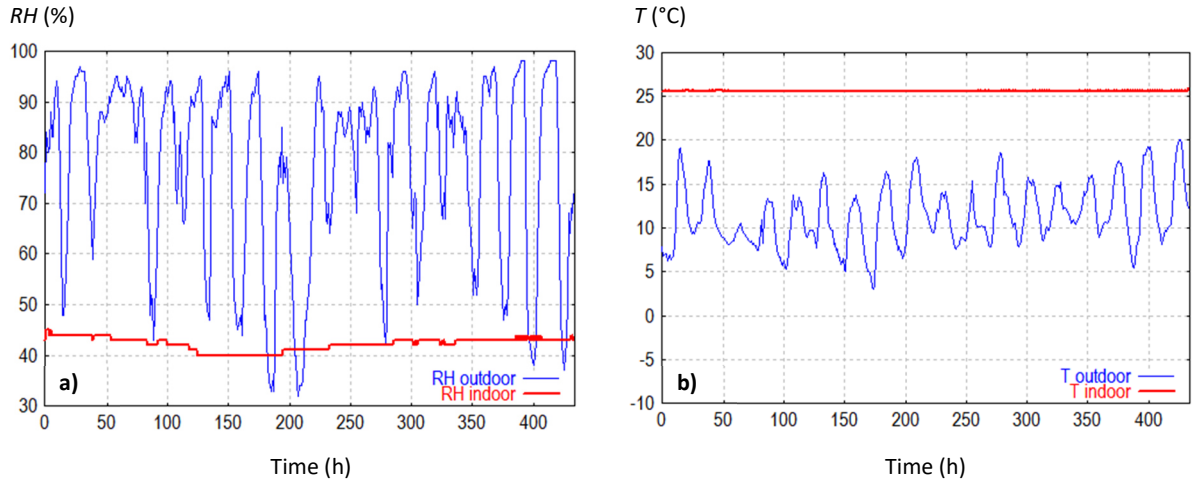

Figure 5: Bordeaux data – Indoor and outdoor *RH* (a) and *T* (b)

4.3.3 Initial conditions

The initial hygrothermal conditions in the wall have been chosen as follows:

- a constant *RH* of 80% in each layer,

- water contents *W* corresponding to *RH* of 80% according to the adsorption isotherm in each layer,

- a constant temperature *T* of 10°C.

Obviously, these initial conditions do not correspond to any realistic situation. Consequently, an iterative procedure has been used to produce a hygric history: the first simulations (with TMC and TMCKIN) have been performed over a full cycle of 18 days considering the aforementioned initial conditions. A second set of simulations have been run again over a full cycle of 18 days considering as initial conditions the final hygrothermal conditions of the first simulations in each layer. Finally, a third set of simulations have been run considering the final hygrothermal conditions of the second simulations in each layer. Only the results of this third set of simulations will be presented here.

4.3.4 Results of the simulations and discussions

The results of the simulations will be investigated in terms of *RH* temporal evolutions at the following positions:

- Position 1 (Pos1): CAV / BIO1 interface,

- Position 2 (Pos2): BIO1 / OSB interface,

- Position 3 (Pos3): INT / BIO2 interface for WCON1, OSB3 / BIO2 interface for WCONF2, OSB4 / BIO2 interface for WCONF3 and WCONF4.

Therefore, the following comparisons in terms of *RH* are fully relevant (if there were high discrepancies, the analysis should have been carried out in terms of vapor partial pressure).

4.3.4.1 Wroughton climate

Figure 6a, 6b and 6c shows the temporal evolution of *RH* at Pos1, Pos2 and Pos3 respectively, from the measurements carried out at the HIVE demonstrator and from the TMC and TMCKIN simulations considering kinetics models (8) and (9). The mean differences between main minima and maxima (*i.e.* mean amplitudes) of the *RH* temporal evolutions have been determined and reported in Table 7 allowing to quantify the small time scale *RH* dynamics.

First, the global level of *RH* at Pos1, Pos2 and Pos3 is reasonably well predicted by the simulations (±5% from measurements). The discrepancies from the measurements may be due to the influence of the actual hygric history which is not known.

Then, it appears that TMC results tend to underestimate the small time scale *RH* dynamics at Pos1 and Pos2: from Table 7, the mean amplitudes are underestimated by 55% and 48% respectively. On the contrary, TMCKIN with model (8) tends to overestimate these mean amplitudes: by 47% and 41% respectively. TMCKIN with model (9) leads to the best results at Pos2 and Pos3 with mean amplitudes in a range of ±15% compared to the measurements. This is clearly in favor of the local kinetics approach described by model (9). At Pos3, all the simulations overestimate significantly the mean amplitudes: the reason of these discrepancies has not been identified.

According to Figures 6d, 6e and 6f, temperature differences between measurements and simulations are broadly lower than 1 K. TMC and TMCKIN simulations lead to the same results (curves coincide in the Figures). As shown in Reuge et al. (2020a), taking into account solar radiation is necessary to obtain a good agreement between measurements and simulations and it allows to obtain an additional contribution of small time scale *RH* dynamics.

The next simulations, performed to compare the different wall configurations, are run with TMCKIN / model (9) because it leads to the best results overall.

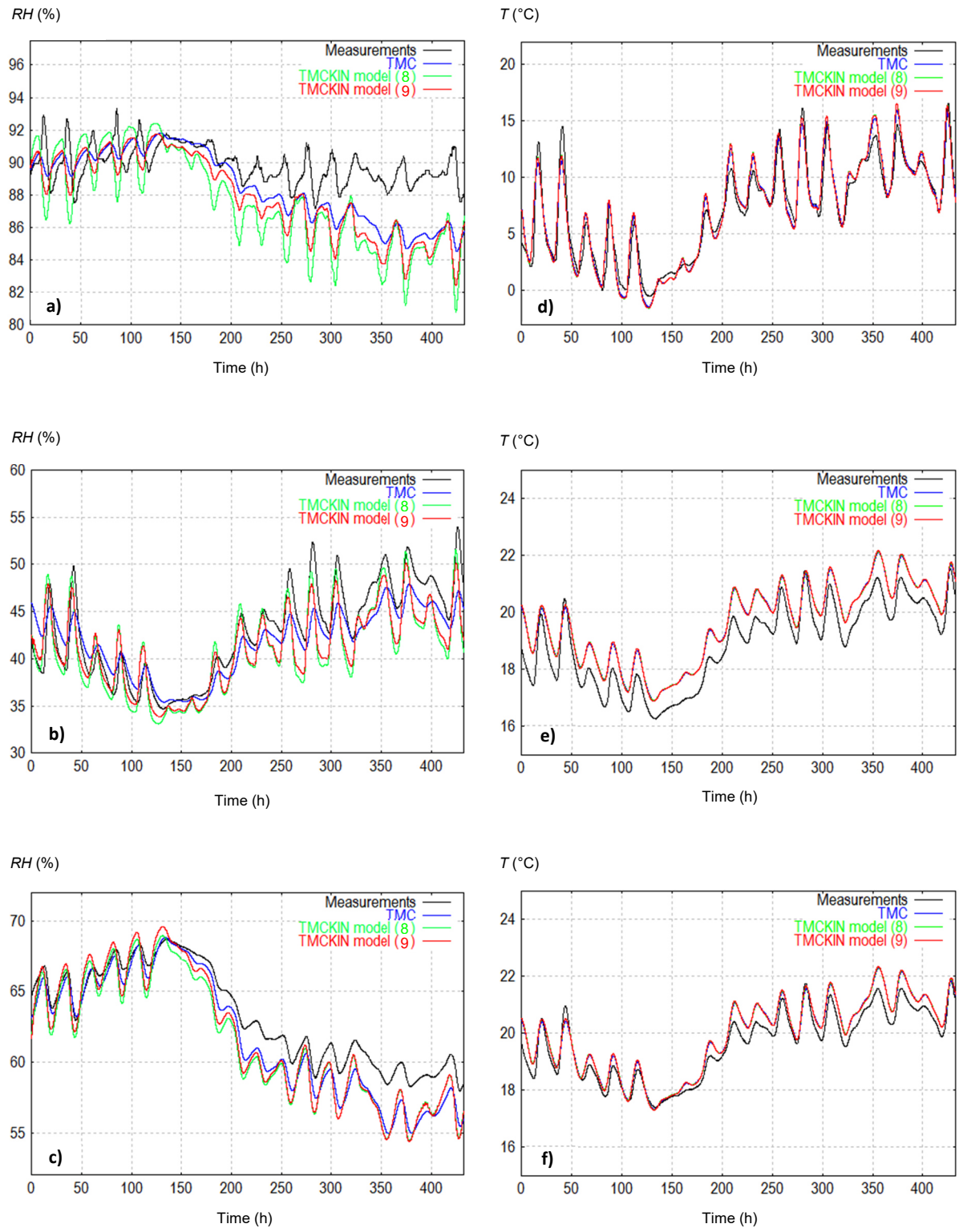

Figure 6: Temporal evolution of *RH* at Pos1 (a), Pos2 (b) and Pos3 (c) and *T* at Pos1 (d), Pos2 (e) and Pos3 (f) – Measurements and simulations (TMC & TMCKIN)

Figure 7 shows the results of the TMCKIN simulations in terms of *RH* temporal evolutions at (a) Pos1, (b) Pos2 and (c) Pos3 for the four wall configurations WCONF1, WCONF2, WCONF3 and WCONF4.

Figure 7a shows that WCONF2 can lead to very high *RH* at Pos1, up to 94%: it can be harmful in terms of durability of the materials subjected to a such high *RH*, bio-based materials being susceptible to mold growth, as shown in several experimental and/or numerical studies (Defo et al., 2021; Fedorik et al., 2021; Gradeci and Berardi, 2019; Viel et al., 2019). Here, this is obviously due to a too low vapor resistance of the wall. For this reason and for the aforementioned reason that WCONF2 air tightness may not be great enough, this wall configuration can be rejected.

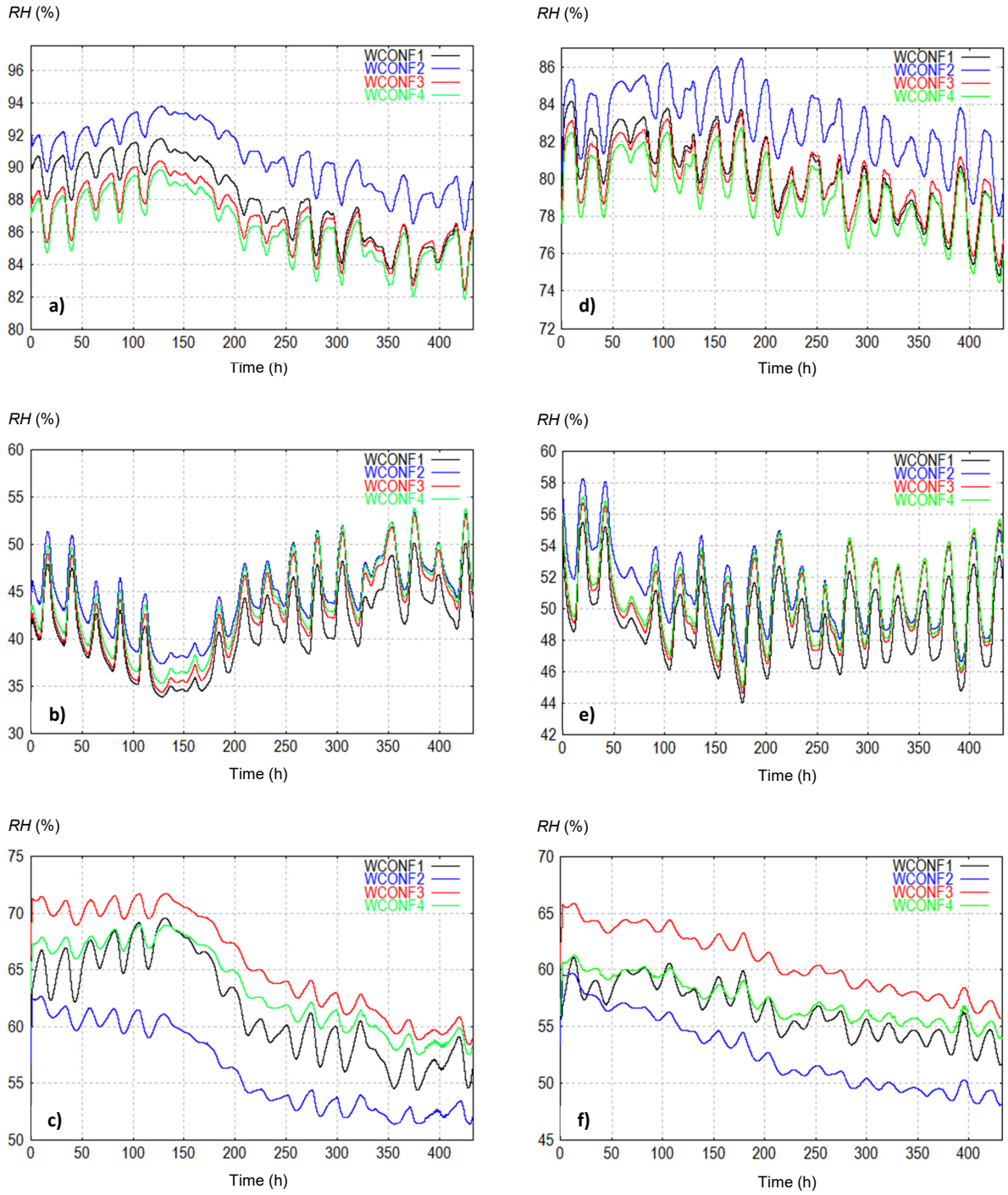

Figure 7: Temporal evolution of *RH* – TMCKIN simulations with Wroughton climate at (a) Pos1, (b) Pos2, (c) Pos3, and with Bordeaux climate at (d) Pos1, (e) Pos2, (f) Pos3, for the different wall configurations

With WCONF3 and WCONF4, *RH* does not exceed 90% (while with WCONF1, it reaches 92%), thus these two last configurations are favorable from this point of view.

At Pos3, Figure 7c and Table 8 show that for WCONF3 and WCONF4 (and WCONF2), the small time scale *RH* fluctuations are lower than those obtained for WCONF1 by a factor of about 2: the removal of INT allows the external layers to play their role of moisture transfer damping; this was expected and this is confirmed by the comparisons of the global water content variations in the external layers (CAV, BIO1 and OSB3 / OSB4): for WCONF3, they are greater than the ones of WCONF1 by about 20%. Temperatures obtained from the simulations of the different configurations lead to very close results (difference lower than 1 K) at the studied positions.

	Pos1	Pos2	Pos3
Measurements	2.76	6.19	2.18
TMC	1.23	3.19	2.66
TMCKIN – model (8)	4.06	8.74	4.14
TMCKIN – model (9)	2.39	7.13	4.06

Table 7: Mean amplitudes of *RH* variations (%) – Reference configuration (WCONF1), Wroughton climate

	Pos1	Pos2	Pos3
WCONF1	2.39	7.13	4.06
WCONF2	1.96	6.94	1.92
WCONF3	2.70	7.71	1.92
WCONF4	2.85	7.78	1.91

Table 8: Mean amplitudes of *RH* variations (%) – TMCKIN model (9), Wroughton climate

4.3.4.2 Bordeaux climate

Figure 7 shows the results of the TMCKIN / model (9) simulations in terms of *RH* temporal evolutions at (d) Pos1, (e) Pos2 and (f) Pos3 for the four wall configurations WCONF1, WCONF2, WCONF3 and WCONF4. At Pos1, *RH* are lower than with the Wroughton's climate but the amplitudes of their variations are greater with a mean value of 2.86%, 2.55%, 3.1% and 3.25% for WCONF1, WCONF2, WCONF3 and WCONF4 respectively. Maximum *RH* does not exceed 86.5% (WCONF2).

As shown by Figure 7d, the small time scale *RH* fluctuations in WCONF2, WCONF3 and WCONF4 at Pos3 are still lower (by a factor up to 2) than those obtained for WCONF1.

At this point of the study, considering the walls behavior against the two studied climates, WCONF3 and WCONF4 reveal to be good candidates to replace the reference wall WCONF1 even if average *RH* is somewhat greater at Pos3.

4.3.4.3 Indoor cyclic loads

The indoor *RH* measured at the HIVE demonstrator and used until now are not representative of a building in real life conditions. From these data, it has been decided to add indoor *RH* cyclic loads which can, for instance, represent the effect of a family taking showers every morning: between 7 a.m. and 8 a.m., indoor *RH* is set to 100%. The temporal evolution of indoor *RH* is showed in Figure 8.

Figure 9 and Table 9 allow to compare the results of TMC / TMCKIN model (8) / TMCKIN model (9) simulations in terms of *RH* temporal evolutions at Pos3 for the wall configuration WCONF1 under the Wroughton climate. It is interesting because it shows that the Künzel approach largely underestimates the *RH* peaks (with a mean amplitude of 2.68) compared to the local kinetics approach.

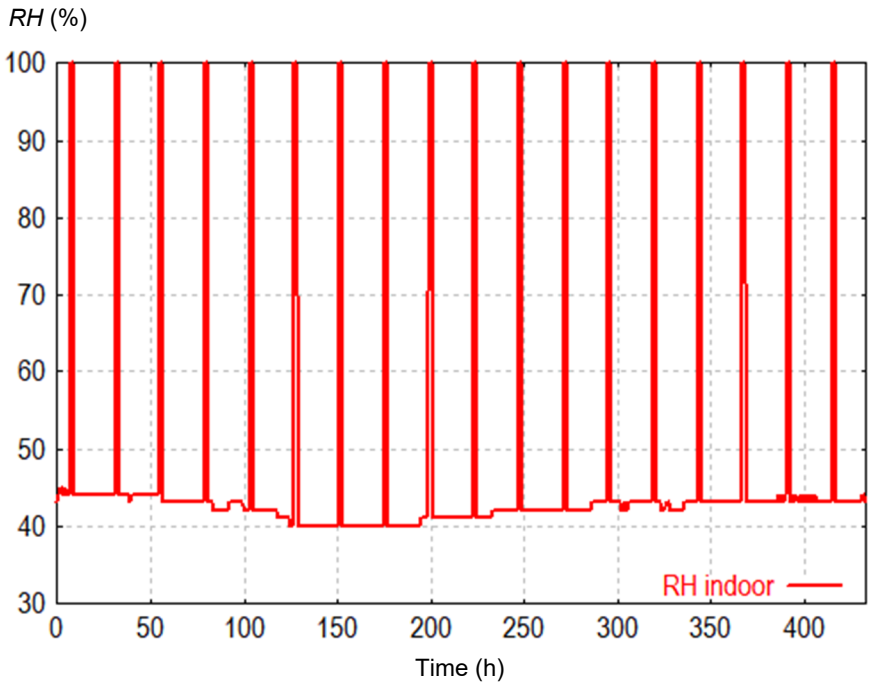

Figure 8: Indoor *RH* with cyclic loads

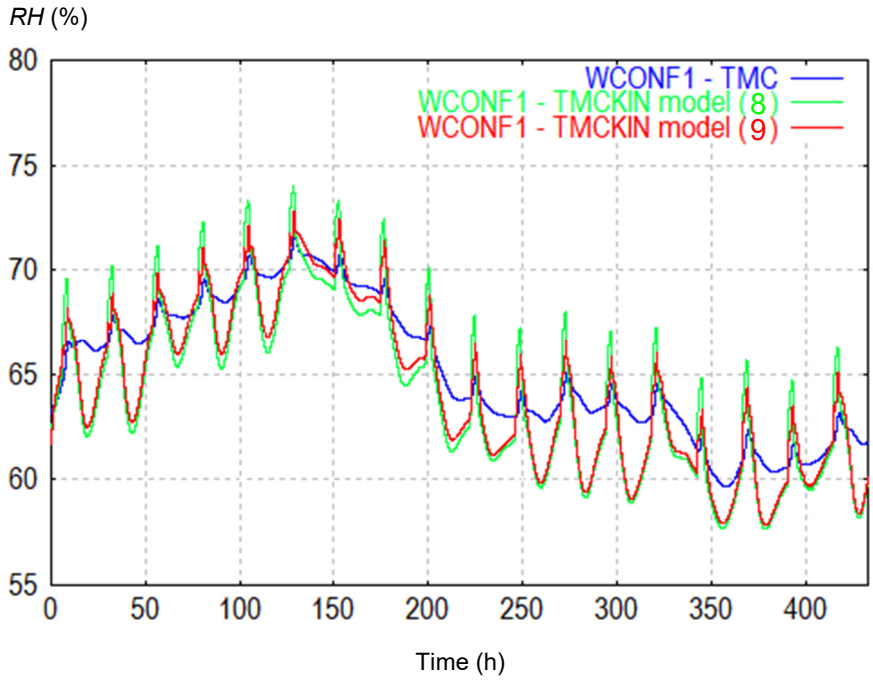

Figure 9: Temporal evolution of *RH* at Pos3 – TMCKIN & TMC simulations – Wroughton climate

Actually, the quasi-infinite kinetics considered by the Künzel approach results in an overestimation of the materials' moisture damping capacity. In comparison with kinetics model (8), kinetics model (9) leads to lower *RH* peaks with mean amplitudes of 7.11% and 5.36% respectively.

Note that the results at Pos1 and Pos2 are not shown, actually they are similar to those obtained without indoor loads because INT+OSB3 acts as a filter to the indoor cyclic loads.

Figure 10 shows the results of the TMCKIN / model (9) simulations in terms of *RH* temporal evolutions at Pos3 for wall configurations WCONF1, WCONF3 and WCONF4, with (a) Wroughton climate and (b) Bordeaux climate. Again, the results at Pos1 and Pos2 are not shown because they are similar to those obtained without indoor loads. From Figure 10 and Table 9, WCONF3 simulation predicts lower *RH* peak amplitudes than WCONF1 simulation by 51%: the removal of INT allows to attenuate them thanks to the role of moisture damping of the external layers; the comparisons of the global water content variations in the external layers (CAV, BIO1 and OSB3 / OSB4) show that for WCONF3, they are greater than the ones of WCONF1 by about 4%.

Then, WCONF4 simulation predicts *RH* peaks higher than WCONF3 simulation by 103% at Pos3. Note that from MBV values, CAV is a much better hygric regulator than CSB (with a MBV of 1.7 against 0.77 g/(m².%*RH*), (Collet et al., 2019)). The comparison of the global water content in CSB layer (WCONF3) / internal CAV layer (WCONF4) shows that their variations are greater in the later than in the former by a factor of about 4; therefore, their moisture regulation capacities are in accordance with their MBV values. The higher *RH* peaks for WCONF3 than for WCONF4 at Pos3 can be explained by the low permeability of CSB (μ = 27) compared to the one of CAV (μ = 5.5): *RH* fluctuations are much more damped by CSB than by CAV. This is very interesting because it demonstrates that the MBV value itself is an insufficient characterization of the moisture regulation of a system at a given position.

From these results, WCONF3 should be preferred over WCONF4.

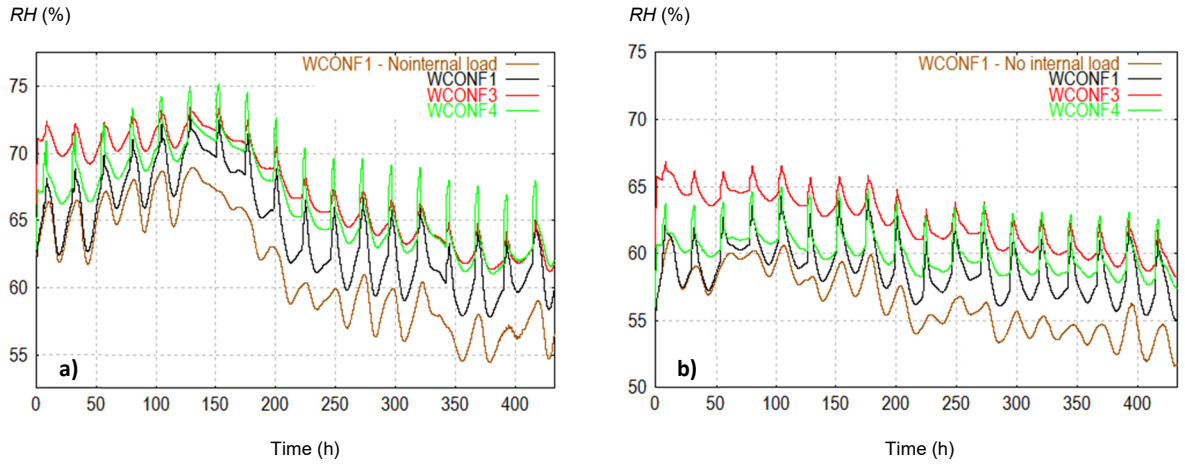

Figure 10: Temporal evolution of *RH* at Pos3 – TMCKIN / model (9) simulations with (a) Wroughton climate and (b) Bordeaux climate for the different wall configurations

	Pos3
WCONF1 - TMC	2.68
WCONF1 – TMCKIN / model (8)	7.11
WCONF1 – TMCKIN / model (9)	5.36
WCONF3 – TMCKIN / model (9)	2.64
WCONF4 – TMCKIN / model (9)	5.56

Table 9: Mean amplitudes of *RH* variations (%) at Pos3 – Wroughton climate

4.3.4.4 Effects of hysteresis

Considering both the adsorption and desorption isotherms of CAV presented in Figure 2 and section 4.2 and considering the hysteretic model of Huang et al. (2005), some further simulations have been performed. When hysteresis is applied to the CAV layer, the corresponding value of μ_{TMCKIN} (*i.e.*, 4.5, *cf*. Table 6) is used.

For WCONF1 subjected to the Wroughton climate, Figure 11a shows the results obtained with TMCKIN / model (9) at Pos1. Compared to the run without hysteresis, global *RH* evolutions are relatively close and the mean amplitude of *RH* variations is slightly greater (by less than 1% *RH*, as shown in Fig. 11b). Thus, under these operating conditions, hysteresis has relatively limited effects on the RH variations but in principle leads to more realistic water content levels.

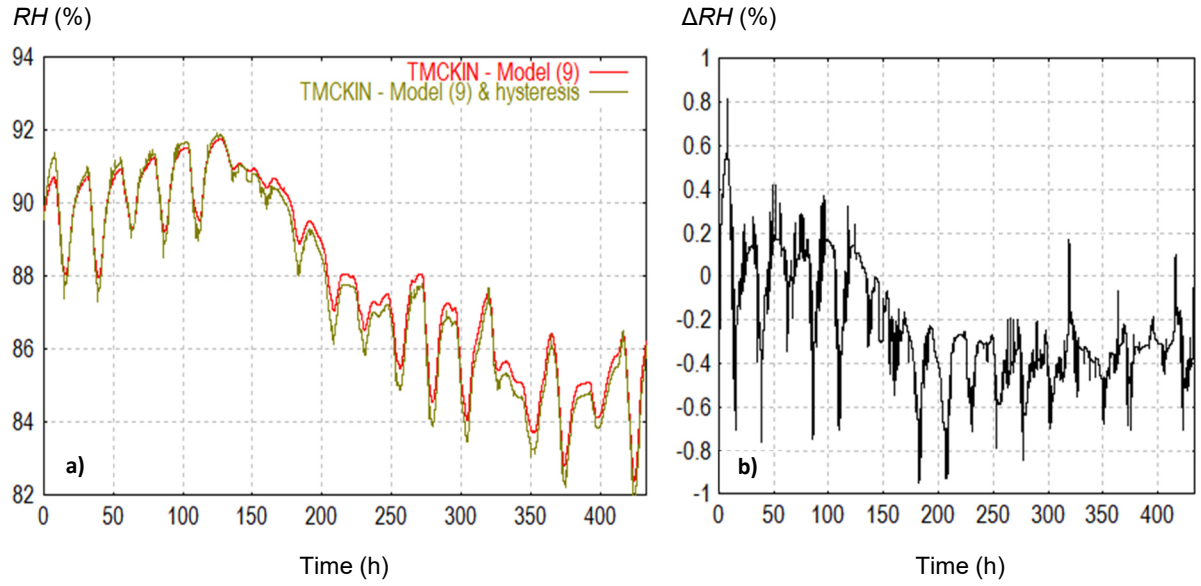

Figure 11: WCONF1, (a) temporal evolution of *RH* at Pos1 – TMCKIN simulations with / without hysteresis – Wroughton climate, (b) temporal evolution of the difference Δ*RH* between the results with hysteresis and the results without hysteresis

For WCONF4, with hysteresis applied to the internal CAV layer, subjected to the Wroughton climate and the indoor cyclic loads, Figure 12a shows the results obtained with TMCKIN / model (9) at Pos3. It appears that the obtained *RH* dynamics is nearly the same as the one obtained without hysteresis, with mean amplitudes differing only by 1.4%, the differences of *RH* variations being lower than 0.5% most of the time as shown in Fig. 12b. Thus, under these operating conditions, provided that the μ values are adequately adjusted beforehand on the MBV tests, simulations with or without hysteresis lead to almost the same results in terms of *RH* dynamics, this is remarkable. It must be emphasized that unlike

the previous run at Pos1, this run at Pos3 remains in the range of operating conditions of the MBV tests (*i.e.*, 33% ≤ *RH* ≤ 75%). This result would require further investigations. On a numerical point of view, since taking account of hysteresis effects involves a certain level of coding complexity, it would be very interesting to support the evidence that it is not necessary under a range of operating conditions.

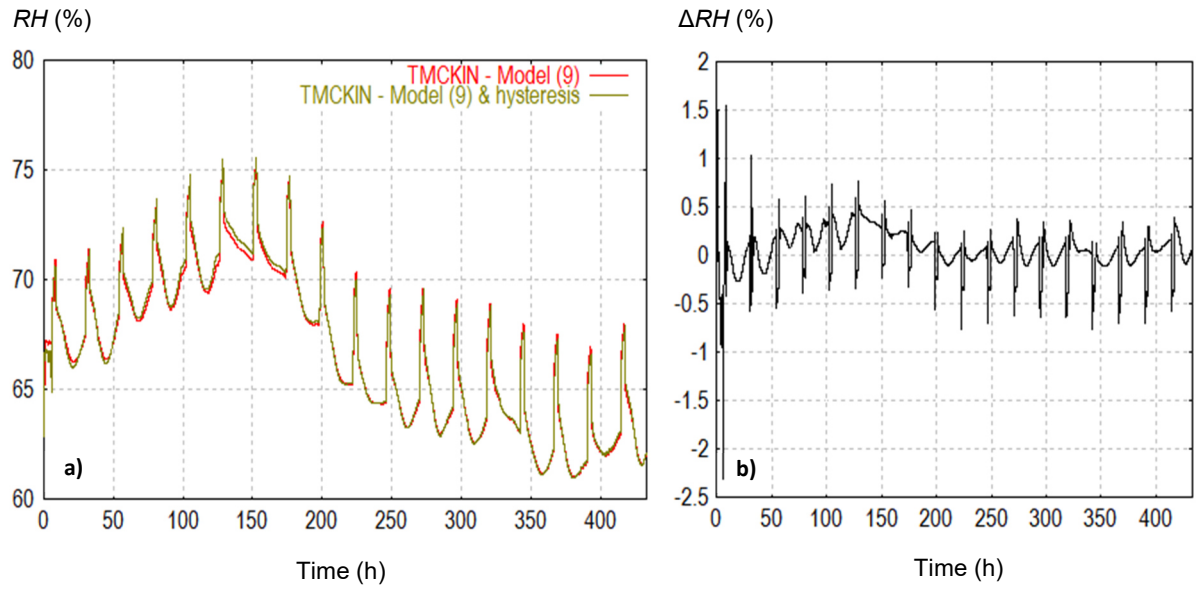

Figure 12: WCONF4, (a) temporal evolution of *RH* at Pos3 – TMCKIN simulations with / without hysteresis – Wroughton climate and indoor cyclic loads, (b) temporal evolution of the difference Δ*RH* between the results with hysteresis and the results without hysteresis

5 Conclusion

Beside the reference ISOBIO wall (WCONF1), three different wall configurations (WCONF2, WCONF3 and WCONF4) have been numerically tested under two climates: Wroughton, UK, Feb-Mar 2018 and Bordeaux, FR, Apr 2008. From the results of the simulations, WCONF2 (same as WCONF1 but without Proclima INTELLO membrane) has to be rejected: it leads to too high *RH* (up to 94%) at the CAV / BIO1 interface resulting in possible mold growth. On the other hand, WCONF3 (OSB3 12 mm + INTELLLO membrane replaced by OSB4 18 mm) seems more favorable than WCONF1: it leads to lower *RH* at the CAV / BIO1 interface and allows to soften more efficiently any indoor cyclic load. Note that WCONF3 increases the moisture damping without any risk of internal condensation. The last studied wall configuration WCONF4 (same as WCONF3 but with CSB replaced with CAV) could be expected to be the best in all points but surprisingly revealed, with the considered assumptions, to be less good intra-wall moisture regulator than WCONF3 against indoor cyclic loads. Actually, the Moisture Buffer Value of a layer is not the only criterion that should be considered in order to ensure hygric performances but strong interaction occurs with its permeability independently of its water sorption capacity.

Moreover, this study has confirmed the differences obtained from calculations based on the classical approach of Künzel (TMC) on one hand and on the local kinetics approach on the other hand (TMCKIN). Although both approaches seem to satisfactorily describe the hygric behavior of samples submitted by Moisture Buffer Value tests, it leads to different adjustments of the samples permeabilities: the

adjustments obtained with TMCKIN with the improved kinetics model globally seem in better adequacies with measurements than those obtained with TMC.

Then, at the wall scale submitted to a real climate, it has been shown that TMCKIN led to better results than TMC as TMCKIN predicts more realistic relative humidity dynamics with greater amplitudes at small time scales at the studied positions. The improved kinetics model used in this study has revealed to be the most consistent with the measurements in terms of relative humidity dynamics and thus able to provide better descriptions of hygric behaviors of the studied bio-based materials.

Finally, water content hysteresis phenomena have been studied at the layers scale. In the considered operating conditions, their effects on the hygric behavior of the wall at the studied positions are quite small from the simulations. Moreover, it appeared that under some operating conditions, they can be ignored formerly by adjusting the layers' permeabilities to adequate fit on the Moisture Buffer Value tests. Since taking account hysteresis effects involves a certain level of coding complexity, it would be very interesting to support the evidence that it is not necessary under a range of operating conditions. This will need to be more deeply investigated in further investigations.

Thus, the numerical investigations have brought many results that were not a priori intuitive and raise into question some presupposed points too easily accepted in the considered field.

Acknowledgments

This work has been performed and funded in the framework of the European project ISOBIO – (http://isobioproject.com) within the scope of the research and innovation program Horizon 2020 (agreement No. 636835). This work has also been supported by the French region Bretagne Loire (UBL).

References

Abbas MS, McGregor F, Fabbri A et al. (2020) The use of pith in the formulation of lightweight bio-based composites: impact on mechanical and hygrothermal properties. *Construction and Building Materials* 259: https://doi.org/10.1016/j.conbuildmat.2020.120573.

Alexandersson M, Askfelt H and Ristinmaa M (2016) Triphasic model of heat and moisture transport with internal mass exchange in paperboard. *Transport in Porous Media* 112: 381–408.

Carmeliet J, De Wit M, Janssen H (2005) Hysteresis and moisture buffering of wood. In: *7th Nordic Symposium on Building Physics*, Reykjavik, Islande.

Challansonnex A, Casalinho J, Perré P (2019a) Non-Fickian diffusion in biosourced materials: Experimental determination of the memory function using minute samples. *Construction and Building Materials* 224: 560–571.

Challansonnex A, Casalinho J, Perré P (2019b) Non-Fickian diffusion in biosourced materials: Prediction of the delay between relative humidity and moisture content. *Energy & Buildings* 202: https://doi.org/10.1016/j.enbuild.2019.109340.

Colinart T, Glouannec P, Bendouma M et al. (2017) Temperature dependence of sorption isotherm of hygroscopic building materials. Part 2: Influence on hygrothermal behavior of hemp concrete. *Energy and Buildings* 152: 42–51.

Colinart T, Lelievre D and Glouannec P (2016) Experimental and numerical analysis of the transient hygrothermal behavior of multilayered hemp concrete wall. *Energy and Buildings* 112: 1–11.

Collet F, Bart M, Serres L et al. (2008) Porous structure and water vapour sorption of hemp-based materials, *Construction and Building Materials* 22: 1271–1280.

Collet F and Pretot S (2014) Thermal conductivity of hemp concretes: Variation with formulation, density and water content. *Construction and Building Materials* 65: 612–619.

Collet F, Pretot S, Colson V et al. (2019) Hygric properties of materials used for ISOBIO wall solution for new buildings. In: *3rd International Conference on Bio-Based Building Materials*, Belfast, UK, June 26th - 28th.

Costantine G, Maalouf C., Moussa T et al. (2020) Hygrothermal evaluation of hemp concrete at wall and room scales: Impact of hysteresis and temperature dependency of sorption curves. *Journal of Building Physics* 44(3): 183-224.

Defo M, Lacasse M, Laouadi A (2021) A comparison of hygrothermal simulation results derived from four simulation tools, *Journal of Building Physics*: https://doi.org/10.1177/1744259120988760.

Dhakal U, Berardi U, Gorgolewski M et al. (2017) Hygrothermal performance of hempcrete for Ontario (Canada) buildings. *Journal of Cleaner Production* 142: 3655-3664.

Douzane O, Promis G, Roucoult JM et al. (2016) Hygrothermal performance of a straw bale building: In situ and laboratory investigations. *Journal of Building Engineering* 8: 91-98.

Eitelberger J and Svensson S (2012) The sorption behavior of wood studied by means of an improved cup method. *Transport in Porous Media* 92: 321–335.

Erhorn H and Szerman M (1992) Überprüfung der Wärme- und Feuchteübergangskoeffizienten in Außenwandecken von Wohnbauten. In: *Gesundheitsingenieur* 113, H. 4, S, pp. 177–186.

Fedorik F, Alitalo S, Savolainen JP et al. (2021) Analysis of hygrothermal performance of low-energy house in Nordic climate. Journal of Building Physics: https://doi.org/10.1177/1744259120984187.

Fabbri A and McGregor F (2017) Impact of the determination of the sorption-desorption curves on the prediction of the hemp concrete hygrothermal behaviour. *Construction and Building Materials* 157: 108–116.

Frandsen HL, Damkilde L and Svensson S (2007) A revised multi-Fickian moisture transport model to describe non-Fickian effects. In *Wood, Holzforschung*, Vol. 61(5), Copyright by Walter de Gruyter, Berlin, New York, pp. 563–572, ISSN 0018-3830.

Fu H, Ding Y, Li M et al. (2021) Research and simulation analysis of thermal performance and hygrothermal behavior of timber-framed walls with different external thermal insulation layer: Cork board and anticorrosive pine plate, *Journal of Building Physics* 45: 180-208.

Gradeci K and Berardi U (2019) Application of probalistic approaches to the performance evaluation of building envelopes to withstand mould groth. *Journal of Building Physics* 43: 187–207.

Huang HC, Tan YC, Liu CW et al. (2005) A novel hysteresis model in unsaturated soil. *Hydrological Processes* 19(8): 1653-1665.

Iglesias HA and Chirife J (1982) *Handbook of Food Isotherms: Water Sorption Parameters for Food and Food Components*. Academic Press Inc., United Kingdom Edition, eBook ISBN: 9780323154277.

Janssen H, Albrecht Scheffler G and Plagge R (2016) Experimental study of dynamic effects in moisture transfer in building materials. *International Journal of Heat and Mass Transfer* 98: 141-149.

Johannesson B and Nyman U (2010) A numerical approach for non-linear moisture flow in porous materials with account to sorption hysteresis. *Transport in Porous Media* 84: 735–754.

Künzel HM (1995) Simultaneous Heat and Moisture Transport in Building Components – One- andTwo-Dimensional Calculation Using Simple Parameters. Report, Fraunhofer IRB Verlag Suttgart, ISBN 3-8167-4103-7.

Lelievre D, Colinart T and Glouannec P (2014) Hygrothermal behavior of bio-based building materials including hysteresis effects: Experimental and numerical analyses. *Energy and Buildings* 84: 617–627.

Mortensen LH, Rode C and Peuhkuri R (2005) *Effect of airflow velocity on moisture exchange at surfaces*. Report, BYG-DTU, Trondheim, ISBN 0-415-41675-2.

Moujalled B, Oumeziane YA, Moissette S et al. (2018) Experimental and numerical evaluation of the hygrothermal performance of a hemp lime concrete building: A long term case study. *Building and Environment* 136: 11–27.

Mnasri F, Bahria S, Slimani MEA et al. (2020) Building incorporated biobased materials: Experimental and numerical study. *Journal of Building Engineering* 28 (2020): available online.

Nyman U, Gustafsson PJ, Johannesson B et al. (2006) A numerical method for the evaluation of non-linear transient moisture flow in cellulosic materials. *International Journal for Numerical Method in Engineering* 66: 1859–1883.

Oumeziane YA (2013) *Evaluation des performances hygrothermiques d'une paroi par simulation numérique : application aux parois en béton de chanvre*. PhD thesis, INSA de Rennes, France.

Oumeziane YA, Bart M, Moissette S et al. (2014) Hysteretic Behaviour and Moisture Buffering of Hemp Concrete. Transport in Porous Media 103: 515-533.

Piot A, Béjat T, Bessette L et al. (2015) Hygrothermal behaviour of a hemp concrete wall: experimental and numerical study of coating. In: *First International Conference on Bio-based Building Materials*, Clermont-Ferrand, France, June 22nd - 24th, e-ISBN: 978-2-35158-154-4.

Rahim M, Tran Le AD, Douzane O et al. (2016) Numerical investigation of the effect of non-isotherm sorption characteristics on hygrothermal behavior of two bio-based building walls. *Journal of Building Engineering* 7: 263–272.

Reuge N, Collet F, Pretot S et al. (2020a) Hygrothermal effects and moisture kinetics in a bio-based multi-layered wall: Experimental and numerical studies. *Construction and Building Materials* 240: available online.

Reuge N, Collet F, Pretot S et al. (2020b) Kinetics of sorption in bio-based materials: theory and simulation of a demonstrator wall. *Proceedings of the Institution of Civil Engineers – Construction Materials*: available online.

Reuge N, Collet F, Pretot S et al. (2020c) Modeling of hygrothermal transfers through a bio-based multilayered wall tested in a bi-climatic room. *Journal of Building Engineering* 32: available online.

Reuge N, Moissette S, Bart M et al. (2019) Water transport in bio-based porous materials: A model of local kinetics of sorption—Application to tree hemp concretes. *Transport in Porous Media* 128(2): 821-836.

Rode C, Peuhkuri RH, Mortensen LH et al. (2005) Moisture buffering of building materials, Technical University of Denmark, Technical report, Department of Civil Engineering.

Schaube H and Werner H (1986) *Wärmeübergangskoeffizient unter natürlichen Klimabedingungen*. Report, IBP-Mitteilung 13, Nr. 109.

Seng B, Lorente S and Magniont C (2017) Scale analysis of heat and moisture transfer through bio-basedmaterials — Application to hemp concrete. *Energy and Buildings* 155: 546–558.

Talev G, Jelle BP, Næss E et al. (2012) Measurement of the convective moisture transfer coefficient from porous building material surfaces applying a wind tunnel method. *Journal of Building Physics* 37 (1): 103–121.

Van Genuchten MT (1980) A closed-form equation for predicting the hydraulic conductivity of unsatured soils. *Soil Science Society of America Journal* 4: 892-898.

Viel M, Collet F, Lecieux Y et al. (2019) Development of a method for assessing resistance to mold growth: application to bio-based composites. In: *3rd International Conference on Bio-Based Building Materials*, Belfast, UK, June 26th - 28th.

Nomenclature

Latin symbols

Cp_0	Specific heat capacity at dry state ($J.kg^{-1}.K^{-1}$)
D_v	Vapor diffusivity in air ($m^2.s^{-1}$)
$D_{v,p}$	Vapor diffusivity in a porous medium ($m^2.s^{-1}$)
$D_{l,p}$	Liquid water diffusivity in a porous medium ($m^2.s^{-1}$)
h	Adjustment coefficient according to eq. (1)
h_m	Mass transfer coefficient ($kg.m^{-2}.Pa^{-1}.s^{-1}$)
k_0	Local kinetic constant defined in eqs. (5, 6) ($day^{-1}/(kg.m^{-3})$)
M_w	Water molar mass ($kg.mol^{-1}$)
P_{sat}	Saturation vapor pressure in air (Pa)
R	Gas constant ($J.mol^{-1}.K^{-1}$)
R_s	Sorption rate ($kg.m^{-3}.s^{-1}$)
RH	Ambient relative humidity or global relative humidity in a sample (-)
S	Sensitivity (-)
T	Temperature (K)
t	Time (s)
w	Local water content ($kg.m^{-3}$)

w_{eq} Local equilibrium water content (kg.m^{-3})

W Global water content in a sample (kg.m^{-3})

W_{eq} Equilibrium water content in a sample (kg.m^{-3})

W_{sat} Maximum water content in a sample (kg.m^{-3})

Greek symbols

β Coefficient defined in eq. (9) (-)

δ_v Vapor permeability of air (kg.Pa^{-1}.m^{-1}.s^{-1})

$\delta_{v,p}$ Vapor permeability of a porous sample (kg.Pa^{-1}.m^{-1}.s^{-1})

ε_0 Porosity (-)

η Adjustment coefficient according to eq. (1)

λ Thermal conductivity (W.m^{-1}.K^{-1})

λ_0 Thermal conductivity at dry state (W.m^{-1}.K^{-1})

λ_a Thermal conductivity of air (W.m^{-1}.K^{-1})

λ_s Adjustment coefficient according to eq. (2)

λ_w Thermal conductivity of water (W.m^{-1}.K^{-1})

μ Vapor diffusion resistance factor (-)

μ_0 Vapor diffusion resistance factor at dry state (-)

φ Local relative humidity (-)

ρ_0 Density at dry state (kg.m^{-3})

Acronyms (ISOBIO materials)

BCB lime-hemp render from BCB™

BIO Biofib Trio flexible insulation panel from CAVAC™

CAV Rigid insulation panel from CAVAC™

CLA Clay-hemp plaster from CLAYTEC™

CSB Lignicell CSB™ panel

OSB Oriented Strand Board

WCONFn Wall configuration n defined in section 2.1